

Supplemental Information

Solution-Based Synthesis and Purification of ZnSnP₂ Nanowires

Erik J. Sheets,^a Robert B. Balow,^b Wei-Chang Yang,^c Eric A. Stach,^d and Rakesh Agrawal*^a

^a *School of Chemical Engineering, Purdue University 480 Stadium Mall Drive West Lafayette, IN 47907.*

^b *Department of Chemistry, Purdue University 560 Oval Drive West Lafayette, IN 47907.*

^c *School of Materials Engineering, Purdue University 701 Stadium Avenue West Lafayette, IN 47907*

^d *Center for Functional Nanomaterials, Brookhaven National Laboratory, 2 Center St., Upton, NY 11973*

Characterization Details

X-Ray Diffraction (XRD)

XRD was conducted using a Rigaku SmartLab. Bragg-Brentano (BB) optics were used with a Cu k-alpha radiation source (40 kV, 40 mA). Background was hardly observed in the measured patterns. Lattice parameters were calculated from the X-ray diffraction (XRD) patterns of the as synthesized nanoparticles using Maud version 2.45. Samples were cast on glass slides and dried prior to scanning.

Transmission Electron Microscopy (TEM) Instrument and Sample Preparation

Transmission electron microscopy was performed on a FEI Tecnai 20 with a LaB₆ filament operating at 200 kV. A silicon drift EDS detector by Oxford Instruments was used in both TEM mode (convergent beam, point by point) and STEM mode at a camera length of 150 mm. STEM-EDS samples were prepared by drop casting the sample from toluene-based dispersion on SiN grids to avoid overlapping X-ray energies between elements in the grid and elements in the sample. High resolution images were obtained from samples dropped on 200-mesh holey carbon on Au grids. SAED images were obtained using a 200 μm select area aperture and a camera length of 150 mm. (S)TEM EDS data was analyzed using Oxford's INCA software.

Raman Spectroscopy

Raman spectroscopy was acquired using a Horiba/Jobin-Yvon LabRAM HR800 confocal microscope with a 633-nm He:Ne laser calibrated using a Si standard.

Gas Chromatography-Mass Spectroscopy (GC-MS)

GC-MS was used to analyze the supernatant from the initial reaction of Zn and Sn with TOP. An Agilent 5975C mass spectrometer system with a typical electron energy of 70 eV and an ion source temperature of 250 °C was used to analyze dilute samples from toluene. Chemical components were separated using a 30 m DB-5 capillary column with an i.d. of 250 μm and a 0.25 μm film thickness. The initial column temperature was 40 °C which heated to 320 °C at 10 °C/min. The injector temperature was set to 250 °C.

Field Emission Scanning Electron Energy Dispersive X-Ray Spectroscopy (FE-SEM EDS)

FE-SEM EDS measurements were obtained from samples applied to carbon tape using an FEI Quanta 3D FEG Dual-beam scanning electron microscope with an Oxford INCA Xstram-2 silicon drift detector operated at an accelerating voltage of 20 kV, spot size 6. Data analysis was performed using Oxford's AZTEC software.

Ultraviolet-Visible Diffuse Reflectance Spectroscopy (DRS)

Diffuse reflectance spectroscopy was performed using a Hitachi U-4100 UV-vis-NIR spectrophotometer (341-F) equipped with an integrating sphere and two detectors (PMT, PbS). The light source was a tungsten lamp (UV-vis) and a deuterium lamp (deep UV). The instrument was operated between 400 and 1400 nm with and without a slit to remove specular reflections and only observe diffuse reflections. Because of the rough surface of the films, spectrums observed with and without the slit were identical indicating a large majority of the incident beam is being scattered rather than reflected like a mirror.

Optically opaque ZnSnP₂ samples were drop cast on glass slides from a sonicated suspension of nanowires in EtOH (200 proof) prior to analysis.

Photoelectrochemical (PEC) Measurements

PEC measurements were performed using a Digi-Ivy D2011 single channel potentiostat equipped with a standard three electrode system consisting of a molybdenum on soda lime glass counter electrode, a Ag/AgCl (4 M KCl) reference electrode, and a tin doped indium oxide (ITO) working electrode. The ZnSnP₂ nanocrystals were dropcast from ethanol onto the ITO substrate and annealed at 250 °C for 15min under nitrogen to help adhere the sample to the substrate. No change was observed in XRD after annealing.

AM1.5G filtered light was produced using a Newport 300 watt Xe arc lamp (Model 66902) calibrated to 100 mW/cm² using an Oriel 91150V silicon reference cell. An IR water filter was used to attenuate the IR portion of light from the solar spectrum to prevent heating of electrolyte during photocurrent measurements.

Sodium sulfide (0.5 M, pH adjusted to 12.0 with HCl) electrolyte was purged with nitrogen gas for at least 1 hr before measuring the photoresponse of ZnSnP₂. A gentle stream of nitrogen was maintained over the top of the photoelectrochemical cell during photocurrent measurements to minimize absorption of oxygen and other potentially reactive gaseous species into the electrolyte. The ZnSnP₂ photoelectrodes were back illuminated with on/off cycles of solar simulated light.

Simultaneous Thermal Analysis (STA)

STA was performed using a TA Instruments SDT Q600 V20.9 Build 20. All experiments were conducted using >10 µg of material, alumina pans, a flow of 200 mL/min He, and a heating of 10 °C/min up to 1000 °C.

Synthesis of Zn_3P_2 and Sn_4P_3 :

Reactions of 1.0 mmol Zn in 20 mmol TOP and 1.0 mmol Sn in 20 mmol TOP were conducted separately to determine the individual effect of each reaction when compared to the combined reaction of Zn, Sn, and TOP. As indicated by XRD, Zn_3P_2 is the product of Zn and TOP while Sn_4P_3 is the product of Sn and TOP when heated to 370 °C for 5hrs. Both these binary phosphides are observed in the combined Zn, Sn, and TOP reaction as well as the target material $ZnSnP_2$.

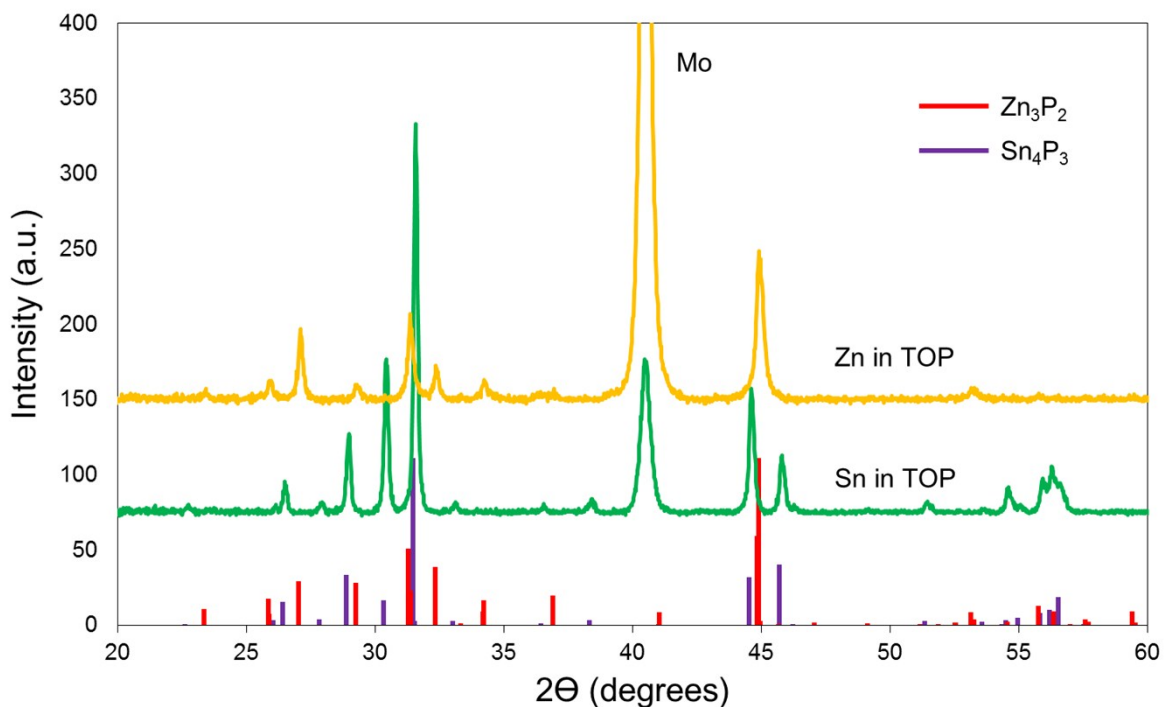


Figure ESI-1. XRD of Zn and Sn reacted individually in TOP showing single phase Zn_3P_2 and Sn_4P_3 respectively.

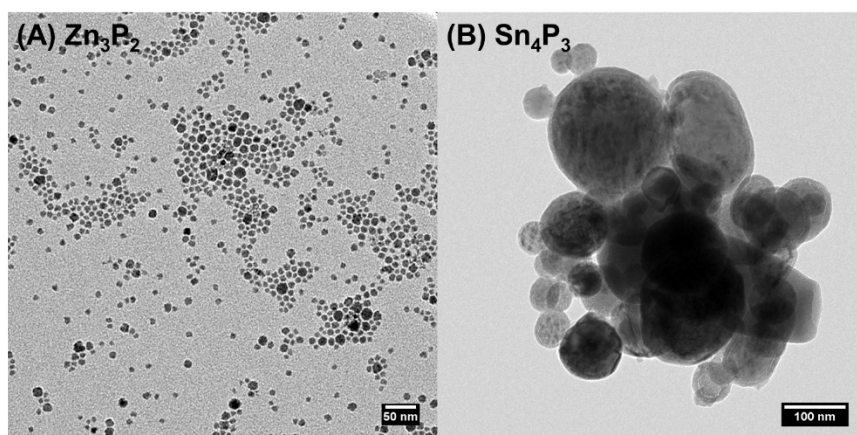


Figure ESI-2. TEM images showing (A) Zn_3P_2 and (B) Sn_4P_3 nanocrystals.

GC-MS Experiments:

GC-MS was conducted on the supernatant after a standard synthesis reaction of Zn and Sn in TOP. The carrier solvent used was toluene. Evidence of TOP as well as a phosphine with one fewer octyl- group support the fact that TOP is decomposing. The oxides are likely attributable to dissolved oxygen in toluene or the handling of the supernatant in air.

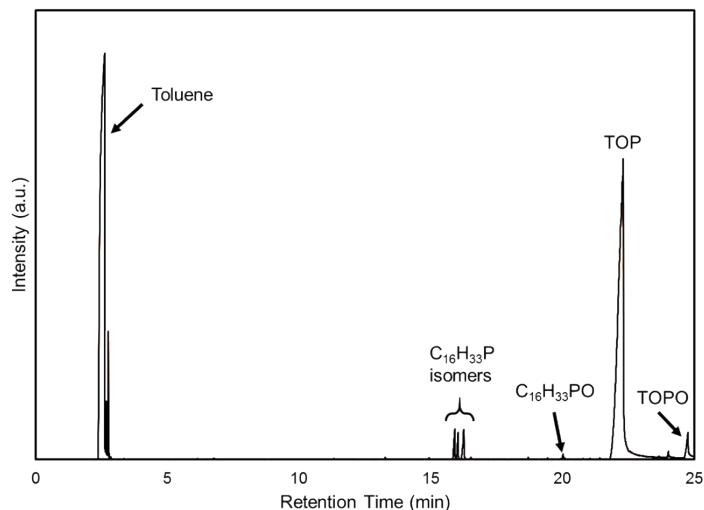


Figure ESI-3. Gas chromatography of the supernatant from the reaction of Zn, Sn, and TOP.

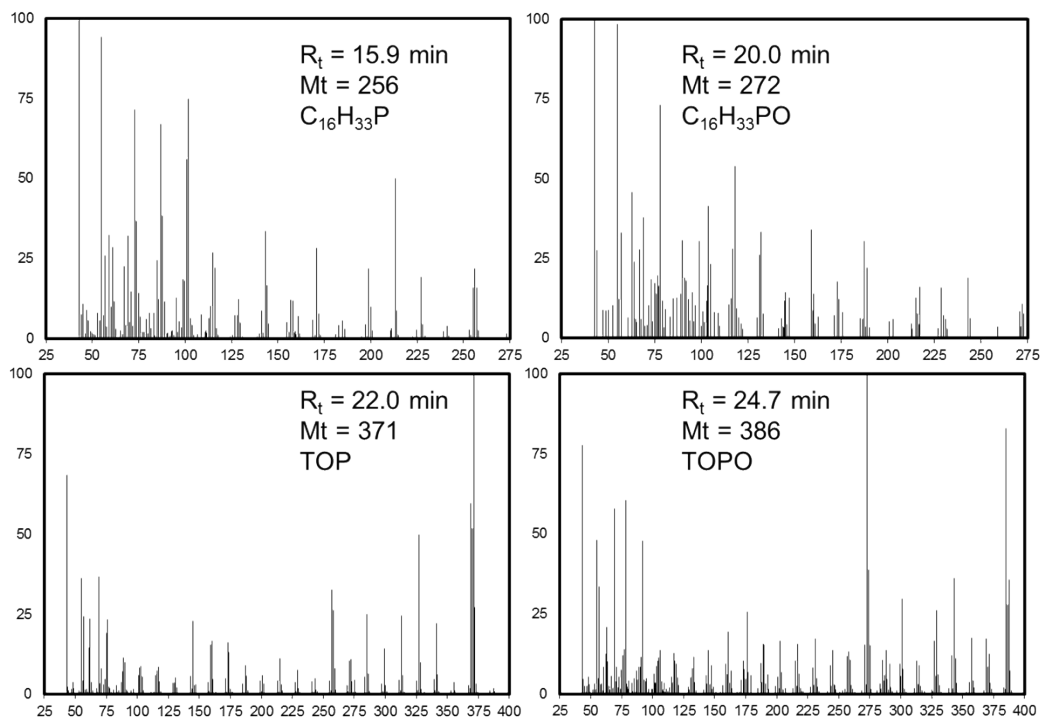


Figure ESI-4. Normalized mass spectrometry of the major peaks observed from gas chromatography above. X-axis is m/z (molecular weight) in all plots.

Optimization of ZnSnP₂ Synthesis Reactions:

To determine the optimal molar ratio of Zn:Sn to make ZnSnP₂ various ratios of Zn:Sn were added to 20 mmol of TOP. Results of XRD are shown below and indicate a stoichiometric 1:1 ratio maximizes the relative peak intensity of ZnSnP₂ compared to the binary phosphide impurity phases. If Zn:Sn is 1:3, SnP_{0.94} (PDF #01-080-1201) is observed along with the expected binary phosphides: Sn₄P₃ and Zn₃P₂. All Samples were cast on molybdenum as a reference peak for baseline corrections. The molybdenum intensity is subject to change depending on the thickness of the film. No peak normalization was conducted.

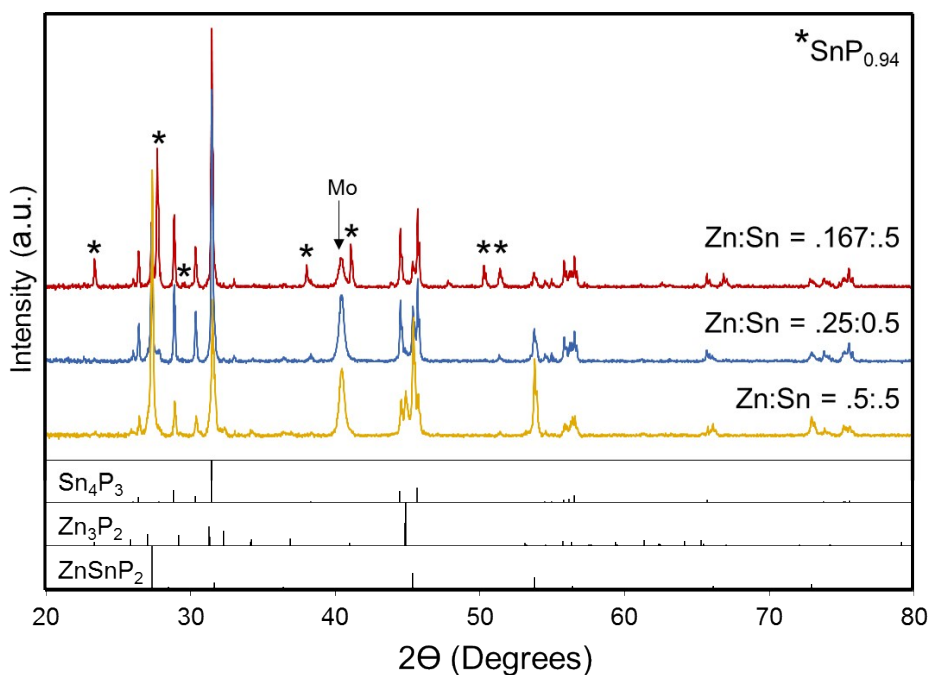


Figure ESI-5. XRD comparison of Zn deficient reactions of Zn, Sn, and TOP together following the standard synthesis. If Zn:Sn is 1:3, Sn_{0.94}P is observed along with the expected binary phosphides: Sn₄P₃ and Zn₃P₂. All samples were cast on a molybdenum substrate as a reference peak.

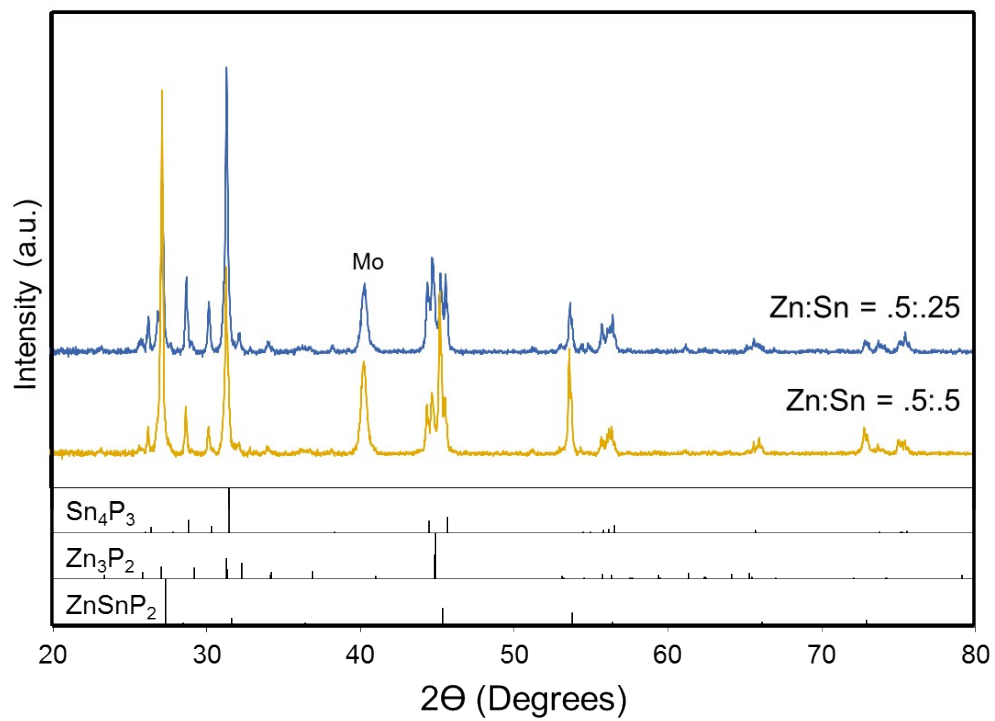


Figure ESI-6. XRD comparison of a Sn deficient experiment where the relative peak intensities of ZnSnP_2 is drastically reduced upon reduction of Sn. Substrate is molybdenum.

Diffuse Reflectance:

Diffuse reflectance was measured on the pure phase ZnSnP₂. To estimate the optical bandgap from the diffuse reflectance spectrum, the measured reflectance was transformed using the Kubelka-Munk function for a fully opaque film.

$$F(R_{\infty}) = \frac{K}{S} = \frac{(1 - R_{\infty})^2}{2R_{\infty}}$$

Here, K is the absorption coefficient; S is the scattering coefficient; and R_∞ is the reflectance of a film whose reflectivity is independent of thickness. A Tauc plot can be generated based on the following relationship:

$$[F(R_{\infty})]^n \propto (h\nu - E_g)$$

Where hν is the energy (eV), n is an index dependent on either a direct (n=2) or an indirect (n=0.5) band transition. The authors would like to make note of a common misinterpretation made frequently when analyzing UV-Vis data: absorption should not be multiplied by energy (hν). Rather, absorption is merely a function of energy.

From Figure 5, a linear regression was generated over the range of 825-953 nm for the direct transition.

	Linear Fit Equation	R ²	X-intercept
Direct Transition	$y = -7.0692 \cdot 10^3 + 9.0908$	0.997	1003.1 nm

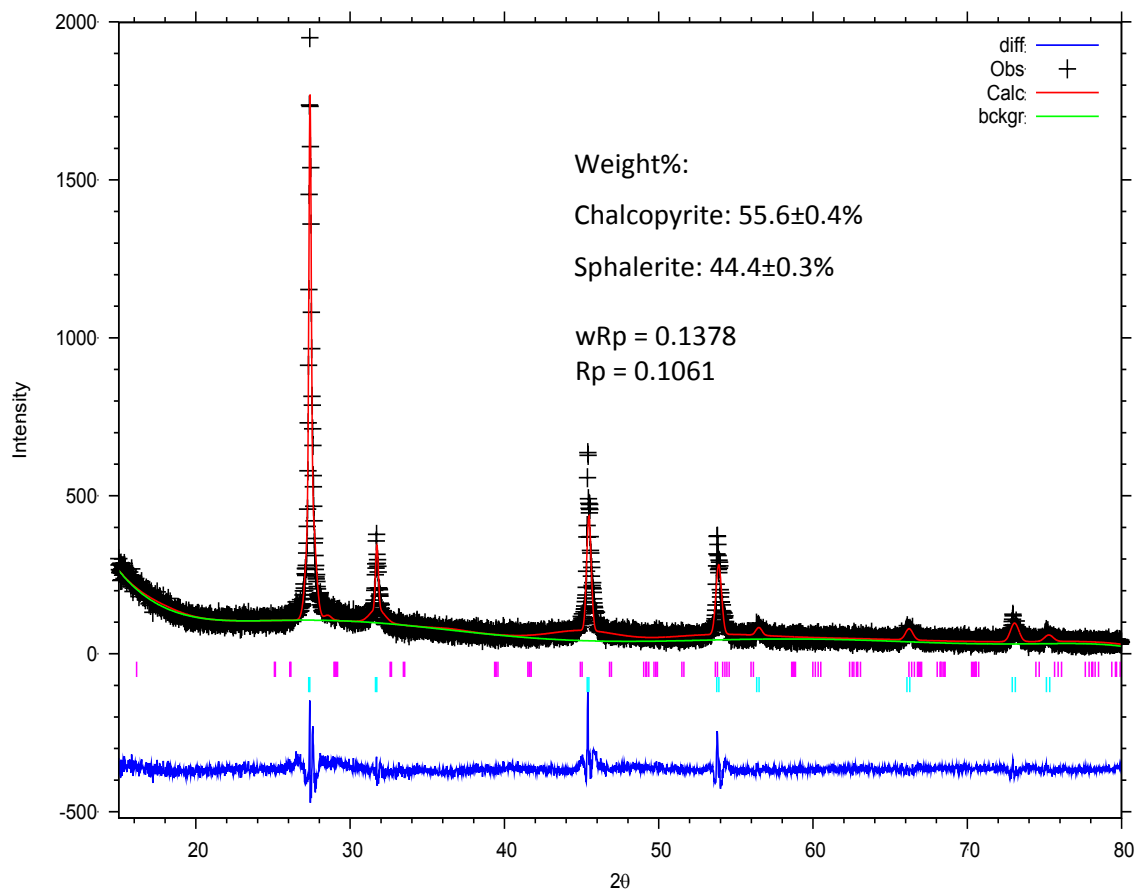


Figure ESI-7. Rietveld refinement of the ZnSnP₂ purified product concluded that the weight fraction of chalcopyrite to sphalerite phases is 55.6 +/- 0.4 % and 44.4 +/- 0.3 % respectively. The fitting parameters wRp and Rp are well within the acceptable ranges for error.

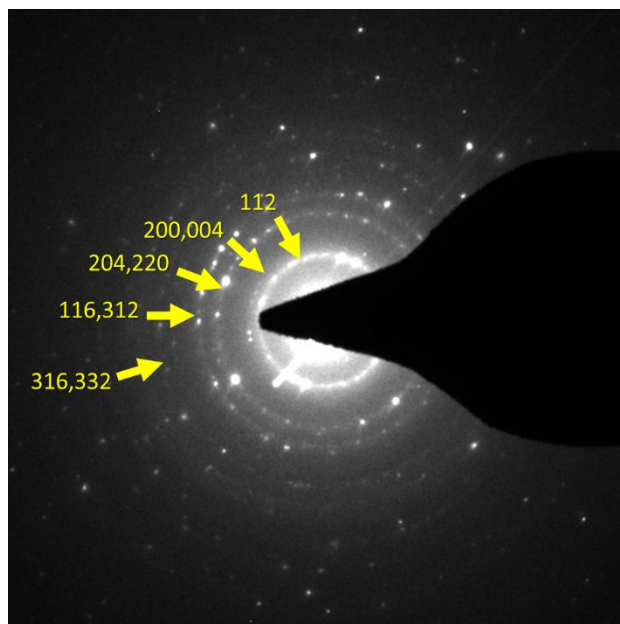


Figure ESI-8. TEM Select area electron diffraction pattern (SAED) of a cluster of purified ZnSnP₂ nanowires (post acid treatment). Camera length is 150 mm using a 200 μm select area aperture.

The ratio of each ring's radius from the SAED were compared to the ratio of d-spacing from the reference chalcopyrite ZnSnP₂ spectrum. Observed ratios indicate the pattern matches ZnSnP₂, and the specific planes were subsequently identified on the SAED pattern.

Planes Compared	Reference Ratio	Observed Ratio
112/200	1.15	1.15
112/204	1.63	1.62
112/116	1.91	1.91
112/316	2.52	2.50

Table ESI-1. Supporting evidence that the ratio of d-spacing from reference planes (PDF# 73-396) matches the observed radius ratios from the SAED pattern in Figure ESI-8 confirming the material is ZnSnP₂.

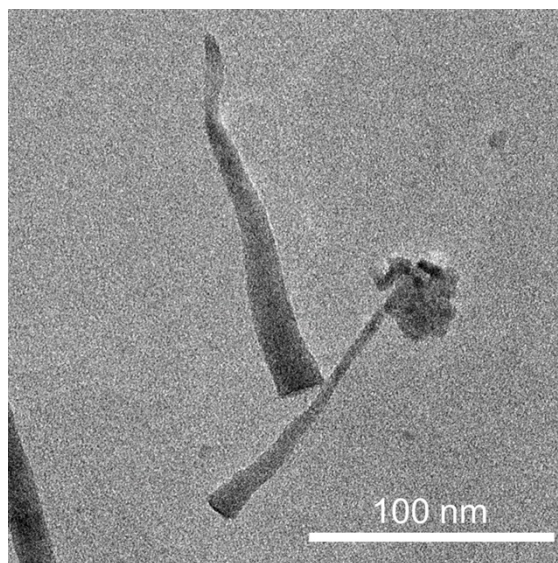
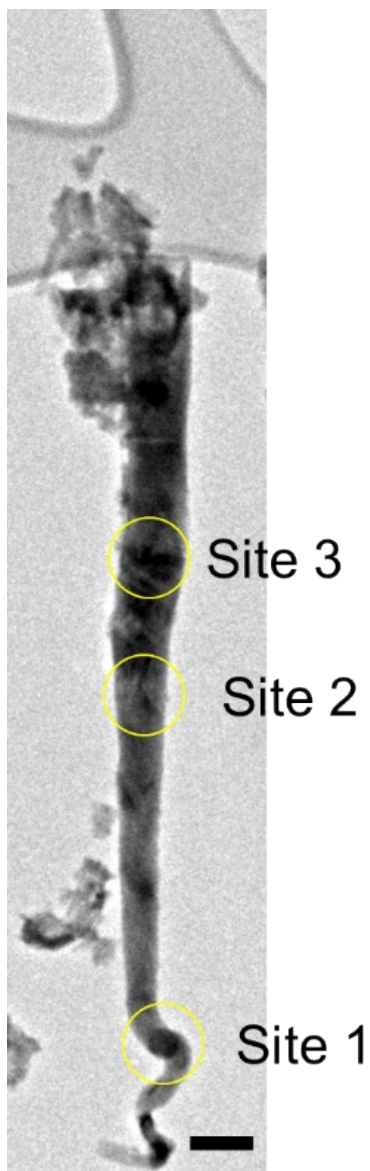


Figure ESI-9. TEM image of Zn nanowires observed after heating a 1 mmol each of Zn and Sn in 1-octadecene at 310 °C for 1 hr. Zn has some solubility in liquid Sn at that temperature and precipitates out as a nanowire upon cooling because the saturation limit is reached at cooler temperatures.



	Zn/P	Sn/P	(Zn+Sn)/P
Site 1	0.36	0.52	0.88
Site 2	0.38	0.54	0.93
Site 3	0.39	0.53	0.92
Average	0.38	0.53	0.91

Figure ESI-10. Table ESI-3. TEM EDS of acid treated ZnSnP_2 showing uniformity across the nanowire and a slight Zn deficiency for this particular nanowire. Scale bar is 100 nm.

Decomposition of Sn_4P_3 through annealing:

In order to show that Sn_4P_3 decomposes into Sn metal and $\text{P}(\text{g})$, we have done STA on a sample of Sn_4P_3 synthesized in the same setup as the synthesis of ZnSnP_2 except the Zn precursor was eliminated (as characterized in Figure ESI-1). The TGA shows a 15% loss in weight which is close to the mass fraction of phosphorus in Sn_4P_3 (16.3%). After the TGA run was complete, the leftover sample was rerun under the same conditions. The DSC analysis of the second run indicates a sharp increase in heat flow into the sample (negative) at the melting point of Sn (230 °C) with no loss in mass. To further confirm the solid left after the decomposition reaction is Sn, a film of Sn_4P_3 was cast from EtOH and annealed at 500 °C for 10 min under 100 sccm Ar. XRD of the annealed Sn_4P_3 showed a single Sn phase present (Figure ESI-12).

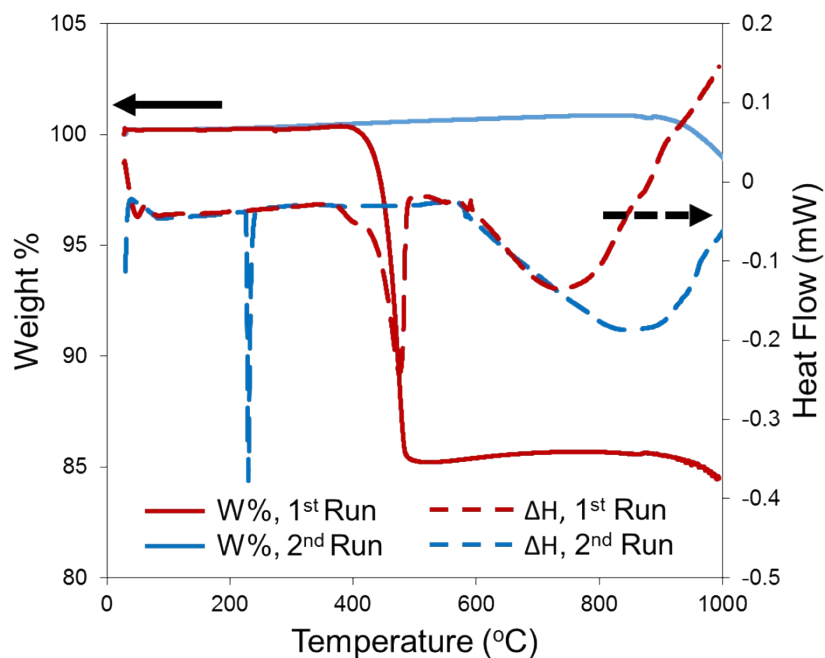


Figure ESI-11. TGA of Sn_4P_3 ran back-to-back showing decomposition of the initial material occurs beginning at 400 °C (red), and the leftover product has a melting point at 230 °C, matching that of Sn. Negative heat flow indicates heating going into the system from the source.

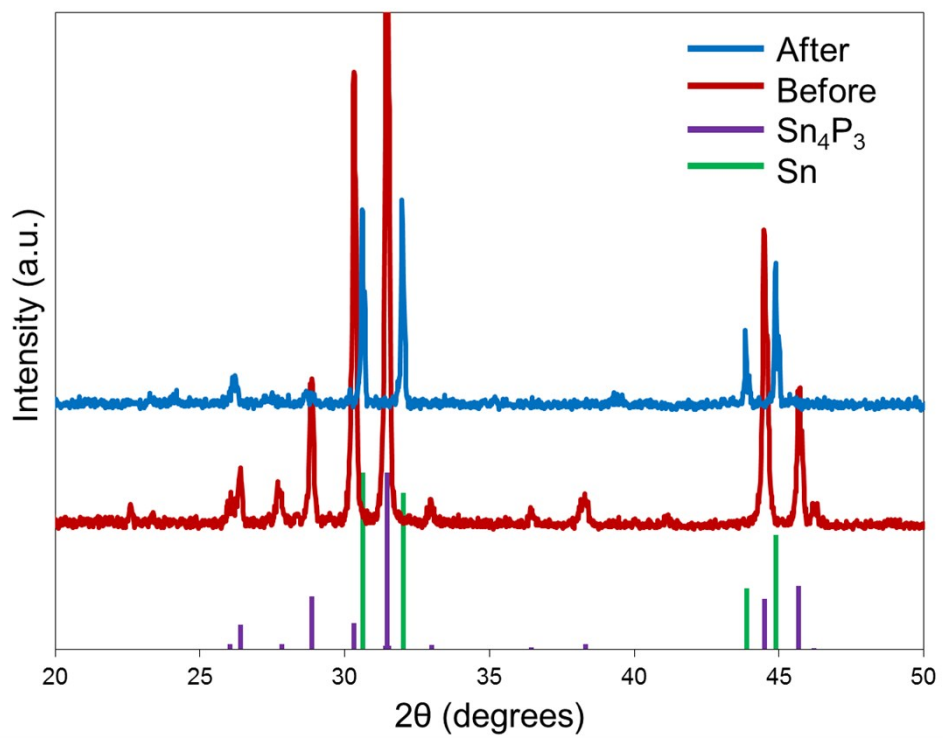


Figure ESI-12. XRD of the as synthesized Sn₄P₃ before (red) and after annealing at 500 °C for 10 min (blue).